Research Article | Vol. 25, No. 26 | 25 Dec 2017 | OPTICS EXPRESS 32581
Optics EXPRESS

Highly sensitive SO_2 photoacoustic sensor for SF_6 decomposition detection using a compact mW-level diode-pumped solid-state laser emitting at 303 nm

XUKUN YIN,[1,2] LEI DONG,[1,2,*] HONGPENG WU,[1,2] HUADAN ZHENG,[1,2] WEIGUANG MA,[1,2] LEI ZHANG,[1,2] WANGBAO YIN, [1,2] LIANTUAN XIAO,[1,2] SUOTANG JIA,[1,2] AND FRANK K. TITTEL[3]

[1]*State Key Laboratory of Quantum Optics and Quantum Optics Devices, Institute of Laser Spectroscopy, Shanxi University, Taiyuan 030006, China*
[2]*Collaborative Innovation Center of Extreme Optics, Shanxi University, Taiyuan 030006, China*
[3]*Department of Electrical and Computer Engineering, Rice University, 6100 Main Street, Houston, TX 77005, USA*
**donglei@sxu.edu.cn*

Abstract: A compact ppb-level SO_2 photoacoustic sensor was developed for the application of SF_6 decomposition detection in electric power systems. The selection of the SO_2 target spectrum is discussed in detail in the infrared (IR) and ultraviolet (UV) spectral regions. Based on the result of the spectrum selection, a small-sized UV-band diode-pumped solid-state laser (DPSSL) emitting at 303.6 nm with an output power of 5 mW was developed. A differential photoacoustic cell (PAC) was designed to match the output optical beam, obtain a high *Q*-factor and reduce the system flow noise in the SF_6 buffer gas. The performance of the sensor system was assessed in terms of gas flow rate, linearity and detection sensitivity. A SO_2 detection limit (1σ) of 74 ppbv was achieved with a 1-s integration time, which corresponds to a normalized noise equivalent absorption (NNEA) coefficient of 1.15×10^{-9} $cm^{-1}WHz^{-1/2}$.

OCIS codes: (280.3420) Laser sensors; (120.4640) Optical instruments; (300.6540) Spectroscopy, ultraviolet.

References and links

1. H. F. Dai, P. Xiao, and Q. Lou, "Application of SnO_2/MWCNTs nanocomposite for SF_6 decomposition gas sensor," Phys. Status Solidi., A Appl. Mater. Sci. **208**(7), 1714–1717 (2011).
2. X. Zhang, B. Yang, X. Wang, and C. Luo, "Effect of plasma treatment on multi-walled carbon nanotubes for the detection of H_2S and SO_2," Sensors (Basel) **12**(7), 9375–9385 (2012).
3. R. Kurte, C. Beyer, H. M. Heise, and D. Klockow, "Application of infrared spectroscopy to monitoring gas insulated high-voltage equipment: electrode material-dependent SF_6 decomposition," Anal. Bioanal. Chem. **373**(7), 639–646 (2002).
4. E. Duffour, "Molecular dynamic simulations of the collision between copper ions, SF_6 molecules and a polyethylene surface: A study of decomposition products and an evaluation of the self-diffusion coefficients," Macromol. Theory Simul. **19**, 88–99 (2010).
5. A. Derdouri, J. Casanovas, R. Hergli, R. Grob, and J. Mathieu, "Study of the decomposition of wet SF_6, subjected to 50-Hz ac corona discharges," J. Appl. Phys. **65**(5), 1852–1857 (1989).
6. J. Olthoff, R. Van Brunt, J. Herron, and I. Sauers, "Detection of trace disulfur decafluoride in sulfur hexafluoride by gas chromatography/mass spectrometry," Anal. Chem. **63**(7), 726–732 (1991).
7. S. Peng, G. Wu, W. Song, and Q. Wang, "Application of flower-like Zno nanorods gas sensor detecting SF_6 decomposition products," J. Nanomater. **2013**(1), 875 (2013).
8. J. Luo, Y. H. Fang, Y. D. Zhao, A. J. Wang, D. C. Li, Y. Y. Li, Y. Liu, F. X. Cui, J. Wu, and J. X. Liu, "Research on the detection of SF_6 decomposition products based on non-resonant photoacoustic spectroscopy," Anal. Methods **7**(3), 1200–1207 (2015).
9. M. W. Sigrist, "Trace gas monitoring by laser photoacoustic spectroscopy and related techniques (plenary)," Rev. Sci. Instrum. **74**(1), 486–490 (2003).

#310167 https://doi.org/10.1364/OE.25.032581
Journal © 2017 Received 27 Oct 2017; revised 7 Dec 2017; accepted 11 Dec 2017; published 14 Dec 2017

Optics EXPRESS

10. H. P. Wu, L. Dong, H. D. Zheng, Y. J. Yu, W. G. Ma, L. Zhang, W. B. Yin, L. T. Xiao, S. T. Jia, and F. K. Tittel, "Calibration-free fast quartz-enhanced photoacoustic spectroscopy based on beat frequency effect for continuous trace gas monitoring," Nat. Commun. **8**, 15331 (2017).
11. X. Yin, L. Dong, H. Zheng, X. Liu, H. Wu, Y. Yang, W. Ma, L. Zhang, W. Yin, L. Xiao, and S. Jia, "Impact of humidity on quartz-enhanced photoacoustic spectroscopy based CO detection using a near-IR telecommunication diode laser," Sensors (Basel) **16**(2), 162 (2016).
12. T. Berer, M. Brandstetter, A. Hochreiner, G. Langer, W. Märzinger, P. Burgholzer, and B. Lendl, "Remote mid-infrared photoacoustic spectroscopy with a quantum cascade laser," Opt. Lett. **40**(15), 3476–3479 (2015).
13. J. Kottmann, J. M. Rey, and M. W. Sigrist, "Mid-Infrared photoacoustic detection of glucose in human skin: towards non-invasive diagnostics," Sensors (Basel) **16**(10), 1663–1677 (2016).
14. P. Patimisco, G. Scamarcio, F. K. Tittel, and V. Spagnolo, "Quartz-enhanced photoacoustic spectroscopy: a review," Sensors (Basel) **14**(4), 6165–6206 (2014).
15. A. Foltynowicz, F. M. Schmidt, W. G. Ma, and O. Axner, "Noise-immune cavity-enhanced optical heterodyne molecular spectroscopy: Current status and future potential," Appl. Phys. B **92**(3), 313–326 (2008).
16. Y. F. Ma, Y. He, L. G. Zhang, X. Yu, J. B. Zhang, R. Sun, and F. K. Tittel, "Ultra-high sensitive acetylene detection using quartz-enhanced photoacoustic spectroscopy with a fiber amplified diode laser and a 30.72 kHz quartz tuning fork," Appl. Phys. Lett. **110**(3), 031107 (2017).
17. H. Yi, K. Liu, W. Chen, T. Tan, L. Wang, and X. Gao, "Application of a broadband blue laser diode to trace NO_2 detection using off-beam quartz-enhanced photoacoustic spectroscopy," Opt. Lett. **36**(4), 481–483 (2011).
18. Z. Wang, Q. Wang, Y. Ching, J. Wu, G. Zhang, and W. Ren, "A portable low-power QEPAS-based CO_2 isotope sensor using a fiber-coupled interband cascade laser," Sens. Actuators B Chem. **246**, 710–715 (2017).
19. Z. Li, Z. Wang, Y. Qi, W. Jin, and W. Ren, "Improved evanescent-wave quartz-enhanced photoacoustic CO sensor using an optical fiber taper," Sens. Actuators B Chem. **248**, 1023–1028 (2017).
20. H. Zheng, M. Lou, L. Dong, H. Wu, W. Ye, X. Yin, C. S. Kim, M. Kim, W. W. Bewley, C. D. Merritt, C. L. Canedy, M. V. Warren, I. Vurgaftman, J. R. Meyer, and F. K. Tittel, "Compact photoacoustic module for methane detection incorporating interband cascade light emitting device," Opt. Express **25**(14), 16761–16770 (2017).
21. L. S. Rothman, I. E. Gordon, Y. Babikov, A. Barbe, D. Chris Benner, P. F. Bernath, M. Birk, L. Bizzocchi, V. Boudon, L. R. Brown, A. Campargue, K. Chance, E. A. Cohen, L. H. Coudert, V. M. Devi, B. J. Drouin, A. Fayt, J.-M. Flaud, R. R. Gamache, J. J. Harrison, J.-M. Hartmann, C. Hill, J. T. Hodges, D. Jacquemart, A. Jolly, J. Lamouroux, R. J. Le Roy, G. Li, D. A. Long, O. M. Lyulin, C. J. Mackie, S. T. Massie, S. Mikhailenko, H. S. P. Müller, O. V. Naumenko, A. V. Nikitin, J. Orphal, V. Perevalov, A. Perrin, E. R. Polovtseva, C. Richard, M. A. H. Smith, E. Starikova, K. Sung, S. Tashkun, J. Tennyson, G. C. Toon, V. G. Tyuterev, and G. Wagner,"The HITRAN 2012 molecular spectroscopic database," J. Quant. Spectrosc. Radiat. Transf. **130**, 4–50 (2013).
22. M. A. Gondal and J. Mastromarino, "Pulsed laser photoacoustic detection of SO_2 near 225.7 nm," Appl. Opt. **40**(12), 2010–2016 (2001).
23. G. Somesfalean, Z. G. Zhang, M. Sjöholm, and S. Svanberg, "All-diode-laser ultraviolet absorption spectroscopy for sulfur dioxide detection," Appl. Phys. B **80**(8), 1021–1025 (2005).
24. H. Keller-Rudek, G. K. Moortgat, R. Sander, and R. Sörensen, "The MPI-Mainz UV/VIS spectral atlas of gaseous molecules of atmospheric interest," Earth Syst. Sci. Data **5**(2), 365–373 (2013).
25. A. Perrin, J. Flaud, A. Goldman, C. Camy-Peyret, W. Lafferty, P. Arcas, and C. P. Rinsland, "NO_2 and SO_2 line parameters: 1996 HITRAN update and new results," J. Quant. Spectrosc. Radiat. Transf. **60**(5), 839–850 (1998).
26. J. P. Waclawek, R. Lewicki, H. Moser, M. Brandstetter, F. K. Tittel, and B. Lendl, "Quartz-enhanced photoacoustic spectroscopy-based sensor system for sulfur dioxide detection using a CW DFB-QCL," Appl. Phys. B **117**(1), 113 (2014).
27. A. R. Whitehill, C. Xie, X. Hu, D. Xie, H. Guo, and S. Ono, "Vibronic origin of sulfur mass-independent isotope effect in photoexcitation of SO_2 and the implications to the early earth's atmosphere," Proc. Natl. Acad. Sci. U.S.A. **110**(44), 17697–17702 (2013).
28. J. Heicklen, N. Kelly, and K. Partymiller, "The photophysics and photochemistry of SO_2," Rev. Chem. Intermed. **3**(3), 315–404 (1980).
29. X. K. Yin, L. Dong, H. P. Wu, H. D. Zheng, W. G. Ma, L. Zhang, W. B. Yin, S. T. Jia, and F. K. Tittel, "Sub-ppb nitrogen dioxide detection with a large linear dynamic range by use of a differential photoacoustic cell and a 3.5 W blue multimode diode laser," Sens. Actuators B Chem. **247**, 329–335 (2017).
30. H. D. Zheng, L. Dong, X. K. Yin, X. L. Liu, H. P. Wu, L. Zhang, W. G. Ma, W. B. Yin, and S. T. Jia, "Ppb-level QEPAS NO_2 sensor by use of electrical modulation cancellation method with a high power blue LED," Sens. Actuators B Chem. **208**, 173–179 (2015).
31. A. Miklós, P. Hess, and Z. Bozóki, "Application of acoustic resonators in photoacoustic trace gas analysis and metrology," Rev. Sci. Instrum. **72**(4), 1937–1955 (2001).
32. H. P. Wu, X. K. Yin, L. Dong, K. L. Pei, A. Sampaolo, P. Patimisco, H. D. Zheng, W. G. Ma, L. Zhang, W. B. Yin, L. T. Xiao, V. Spagnolo, S. T. Jia, and F. K. Tittel, "Simultaneous dual-gas QEPAS detection based on a fundamental and overtone combined vibration of quartz tuning fork," Appl. Phys. Lett. **110**(12), 121104 (2017).
33. J. P. Besson, S. Schilt, and L. Thévenaz, "Multi-gas sensing based on photoacoustic spectroscopy using tunable laser diodes," Spectrochim. Acta A Mol. Biomol. Spectrosc. **60**(14), 3449–3456 (2004).

Optics EXPRESS

34. X. K. Yin, L. Dong, H. P. Wu, W. G. Ma, L. Zhang, W. B. Yin, X. L. Tuan, S. T. Jia, and F. K. Tittel, "Ppb-level H_2S detection for SF_6 decomposition based on a fiber-amplified telecommunication diode laser and a background-gas-induced high-*Q* photoacoustic cell," Appl. Phys. Lett. **111**(03), 031109 (2017).
35. A. Schmohl, A. Miklós, and P. Hess, "Detection of ammonia by photoacoustic spectroscopy with semiconductor lasers," Appl. Opt. **41**(9), 1815–1823 (2002).
36. A. Schmohl, A. Miklós, and P. Hess, "Effects of adsorption-desorption processes on the response time and accuracy of photoacoustic detection of ammonia," Appl. Opt. **40**(15), 2571–2578 (2001).

1. Introduction

In electric power systems, sulfur hexafluoride (SF_6) has been widely used as an insulating medium in gas circuit breakers (GCBs), gas-insulated switchgears (GIS), transformers (GIT), and transmission pipes (GIL) since pure SF_6 gas is noninflammable and highly reliable due to its chemical inertness. Due to the presence of electric arcs, sparks or coronas in electric power systems, SF_6 can be decomposed via the electronic, thermal and optical processes into sulphur fluorides (SF_2, SF_3 and SF_4), which in turn react with electrodes and gas impurities (trace amounts of air and water vapor) to form various chemically active by-products (such as SOF_4, SOF_2, SO_2F_2, SO_2, CO and H_2S). The composition and decomposition rates vary with changing insulating defects. The accumulation of these by-products has led to concerns regarding personnel safety and material compatibility problems. The monitoring of decomposed by-products is able to identify and determine the occurrence of fault types in electrical equipment and thus minimize security risks. It is well known that the formation of sulfur dioxide (SO_2) content is caused by decomposition mechanisms of corona discharges and sparks [1–7]. When the SO_2 concentration is > 8 ppm, the power equipment must be serviced [8]. Therefore, it is critical to develop a sensitive, selective, and cost-effective SO_2 sensor in a SF_6 buffer gas environment for high voltage electric power systems.

Gas sensors have been developed to detect SF_6 decomposition components, such as electrochemical sensors [5], gas detection tubes [2], gas chromatography sensors [6] and semiconductor sensors [7]. However, most of these sensors require a long response time and the detection reliability depends on the environment conditions. Furthermore, these sensors are not suitable for real time monitoring. Recently, trace gas sensors based on laser absorption spectroscopy (LAS) techniques are widely used due to their high detection sensitivity and selectivity, their fast response time as well as their cost effectiveness [9–13]. In 2002, Kurte *et al.* [3] employed a Fourier transform infrared (FTIR) spectrometer to monitor the SF_6 decompositions without concentration quantification. In 2015, Luo *et al.* [8] developed a non-resonant photoacoustic spectroscopy (PAS) sensor with an infrared (IR) radiation source to detect CO, SO_2 and CF_4 continuously with minimum detection limits of 5.9, 8.3 and 5.5 ppm, respectively for CO, SO_2 and CF_4. Although a sensitivity requirement of <1 ppm for SO_2 detection in SF_6 decomposition analysis is more advantageous, a further sensitivity improvement is challenging in the IR spectral region due to a cross-response of SO_2 with SF_6 at high concentration levels (see Section 2).

A special feature of the laser-induced PAS technique is the excitation wavelength independence between the optical source and the photoacoustic signal, which means that any type of laser can be employed in PAS-based sensors, regardless of the excitation optical source wavelengths [14–19]. The PAS technique is based on the targeted molecular absorption of the optical energy, which results in the excitation of molecular energy levels (rotational, vibrational and electronic energy levels). The excited state loses its energy by radiation processes, in which case acoustic waves are generated due to localized transient heating and expansion. Subsequently, photoacoustic transducers (e.g., microphones, quartz tuning forks or fiber tips) are used to detect the pressure fluctuations in a PAS cell [20]. For many atoms and molecules (such as SO_2, NO_2 and O_3), the ultraviolet (UV) spectral region is important to the PAS technique due to the fact that the line strengths of electronic transitions are several orders of magnitude larger than those of ro-vibrational transitions in the IR spectral region [21]. In 2001, Gondal *et al.* [22] used a pulsed laser operating near 225.7 nm

Optics EXPRESS

to detect SO_2 with a detection limit of 1.3 ppbv. In 2005, Somesfalean *et al.* [23] used a tunable UV laser in the wavelength range between 302 nm and 303 nm with an output power of 6.9 nW for SO_2 detection. In this case, the detection limit was ~20 ppmv at atmospheric pressure. However, these gas sensors were bulky owing to the size of the UV lasers, which were designed to operate in a nitrogen (N_2) buffer gas environment. Several SF_6 physical constants (density, thermal conductivity, molar mass, specific heat, viscosity, *et al.*) determine the generation of photoacoustic signal in the PAS, and strongly differ from those applicable to N_2. Hence, these gas sensors are unsuitable to apply to electric power systems.

In this work, we report the development of a highly sensitive SO_2 photoacoustic sensor for the application of SF_6 decomposition detection in an electric power system. A small-sized UV-band diode-pumped solid-state laser (DPSSL) emitting at 303.6 nm with an output power of 5 mW was employed, whose wavelength corresponds to a strong interference-free electronic spectrum of SO_2. A differential photoacoustic cell (PAC) was designed to obtain a high *Q*-factor and reduce the system flow noise. The new optical source, a novel PAC design and strong target spectrum resulted in a ppb-level SO_2 minimum detection limit.

2. Selection of SO_2 detection wavelength and excitation optical source

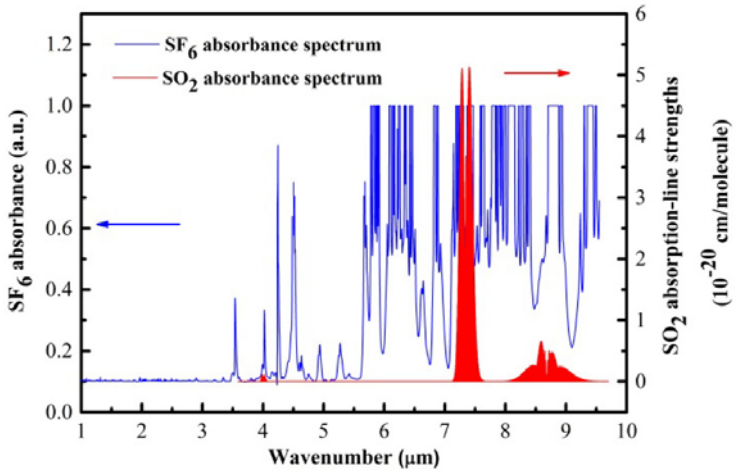

Fig. 1. Pure SF_6 absorbance spectra (blue line) observed by a FTIR spectrometer with a 10 cm gas cell (spectral resolution 0.5 cm^{-1}). SO_2 absorbance spectra (red line) according to the HITRAN database (at 296 K and atmospheric pressure).

The SO_2 molecule shows several strong absorption bands in the IR and UV spectral regions according to the HITRAN database and the MPI-Mainz database, respectively [21, 24]. The HITRAN database indicates that the SO_2 IR absorption bands are located in six different spectral regions (2.5 μm, 3.7 μm, 4 μm, 7.3 μm, 8.6 μm and 19.3 μm), which correspond to the bands $3\nu_3$, $2\nu_3$, $\nu_1 + \nu_3$ and $\nu_1 + \nu_2 + \nu_3$-ν_2, ν_3, ν_1, ν_2 [25]. The 7.3μm region is the strongest IR band of SO_2 corresponding to the fundamental ν_3 band, which is the optimum spectral region for the SO_2 detection in N_2 and air [26]. However, some weaker unidentified absorption bands of SF_6 between 3.3 μm and 10 μm cannot be disregarded in the case of high SF_6 concentration levels since the concentration of SF_6 in an electric power system is usually >99.8%. The HITRAN database includes only the strong ν_3 band of $^{32}SF_6$ at 10.5 μm. To obtain the entire SF_6 spectra for the high concentration levels, a Fourier transform infrared spectroscopy (FTIR) spectrometer (Thermofisher Nicolet IS50) equipped with a transmission cell of 10 cm path length was used. Figure 1 depicts the absorption spectra of pure SF_6 (99.99%) at atmospheric pressure. The same experiment was carried out for 50 ppm SO_2:N_2 and no SO_2 absorption spectra were observed due to the insufficient detection sensitivity of the FTIR. The line position and strength of SO_2 are also plotted in Fig. 1 based on the

Optics EXPRESS

HITRAN database. It is evident that the SO_2 absorption bands in the IR spectral region overlapped with the SF_6 absorption spectra. The SO_2 detection in the IR spectral region is interfered by the strong SF_6 photoacoustic signal and therefore a sensitivity of <1 ppm is difficult to achieve. Hence, the IR spectral region is not an optimal selection for highly sensitive SO_2 detection in a SF_6 buffer gas.

In the wavelength region between 1 and 3 μm, strong absorption bands of SF_6 were not observed, as shown in Fig. 1. In fact, the UV spectral region between 250 nm to 400 nm is also transparent for SF_6 molecules [24]. However, SO_2 exhibits three main absorption band systems in the UV spectral region as shown in Fig. 2: 1. a second allowed band at 165-240 nm ($^1B_2 \leftarrow {}^1A_1$), which is the strongest, 2. a first allowed band at 240-340 nm ($^1A_2$, $^1B_1 \leftarrow {}^1A_1$) and 3. a weak forbidden band at 340-400 nm ($^3B_1 \leftarrow {}^1A_1$), which is not shown [27,28]. H_2S occurs with an unresolved and strong electronic absorption band in the UV spectral region between 160 nm and 250 nm as shown in Fig. 2. In order to avoid cross-talk and obtain a high detection sensitivity, the optimal wavelength region for the SO_2 detection in the SF_6 buffer gas was identified to lie between 250 and 320 nm [29,30].

To reach the optimal detection wavelength region a continuous wave (CW) UV-band DPSSL (Changchun New Industries Optoelectronics Technology Co., Ltd. UV-F-303-nm) with small dimensions of 25 cm × 8.8 cm × 7.4 cm was utilized as the excitation optical source. The solid state laser has an emission wavelength of 303.6 nm and a maximum CW output power of 5 mW at the room temperature. An optical spectrum analyzer (Avantes, AVS-DESKTOP-USB2) was used to measure the emission spectrum of the laser, which is depicted in the inset of Fig. 2. The measured laser linewidth (FWHM) is <0.2 nm.

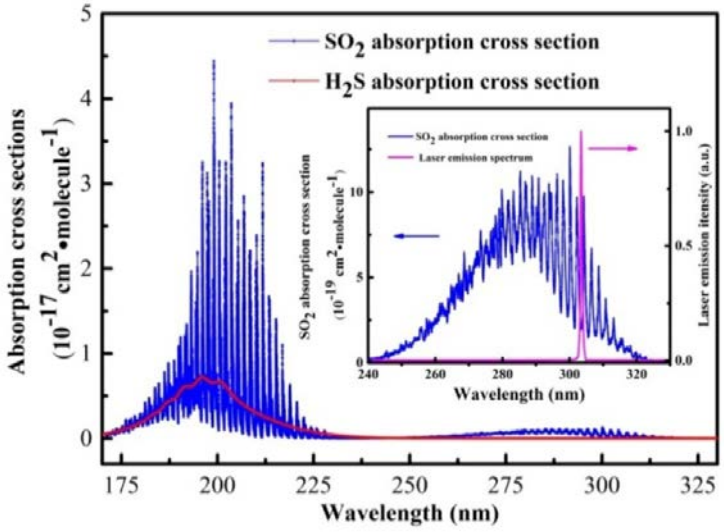

Fig. 2. SO_2 (blue) and H_2S (red) absorption bands between 170 nm-330 nm. Inset: higher resolution absorption spectrum of the first allowed band of SO_2 (blue), and the spectral emission of the DPSSL (magenta).

Subsequently, an experiment of beam quality analysis was carried out since the design of the PAC depends on the beam quality of the excitation optical source. A scanning-slit optical beam profiler (THORLABS BP209-VIS) was placed at a distance of 15 cm from the laser beam exit to image the laser beam profile (see the photos shown in Fig. 3). The energy distribution of the laser is close to a TEM_{00} mode and the output laser beam has a Gaussian-like beam profile with a quality factor $M^2 = 1.51$. The dimension of the ellipsoid shaped laser spot is ~4.5 mm × 2.5 mm. The beam divergence was < 2 mrad (full angle).

Optics EXPRESS

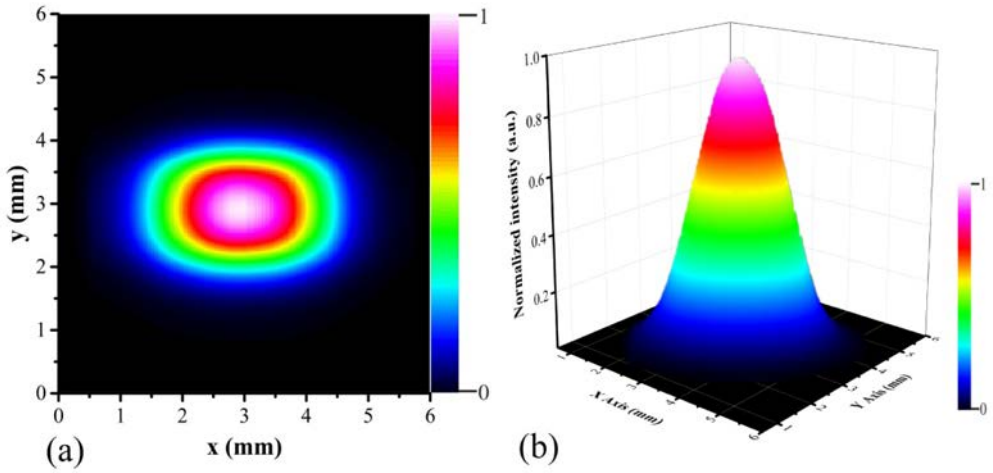

Fig. 3. (a) Two-dimensional intensity distribution of the CW UV-band DPSSL laser beam. (b) Three-dimensional laser beam profile.

3. Photoacoustic cell design

A trace gas sensor based on the PAS technique is a calorimetric method in which the optical energy absorbed in a gas sample is directly measured due to the heating induced in the targeted medium. With a resonant PAC, the modulation frequency is tuned to one of the cell eigenresonances. The detected signal amplitude of microphone *S* can be expressed by Eq. (1) [31–33]:

$$S = C \times P \times \alpha \tag{1}$$

where the proportional factor *C* is termed the cell constant, which describes the photoacoustic resonator sensitivity at its resonance frequency, *P* is the incident radiation power, and α is the absorption coefficient of the targeted gas. According to Eq. (1), a stronger absorption line and a higher power laser are desirable in order to achieve a large signal amplitude and therefore a better detection sensitivity. However for a specific absorption line and a given laser output power the improvement of the cell constant is the only means. An efficient method to increase the cell constant is to use a high-*Q* cell, since the cell constant is proportional to the quality factor (*Q*-factor) [31].The other factor affecting the sensitivity is the noise level. The SF_6 molecules are heavy with a density of 6.12 g/L at sea level conditions, considerably higher than the density of air (1.225 g/L). As a result the gas flow noise caused by the friction between SF_6 molecules and resonator wall is significantly higher than that of N_2. The gas flow rate of SF_6 must be of the order of <20 sccm in order to yield an acceptable flow noise. Such a low flow rate decreases the gas exchange rate and increases the sensor response time in a continuous field measurement.

To reduce the influence of the flow noise in a high-*Q* resonant cell, a PAC with symmetrical differential structure was designed. Two identical cylindrical acoustic resonators (Φ6 × 90 mm in size) were operated in parallel. Two buffer volumes (Φ20 × 10 mm) were added at both ends of the resonators to constitute two identical open-open resonators. At the outside of the buffer volumes, two quartz windows (Φ25.4 × 5 mm) and two rubber O-type rings were used to seal the PAC. The two electret condenser cylindrical microphones have a dimension of Φ6 × 10 mm with a sensitivity of –32 dB, which are installed in the middle of each resonator connecting to the resonator interior via two 1-mm diameter holes. The microphone pair is carefully chosen to have exactly similar response sensitivities. The weaker current signal of each microphone was sent to a custom-made differential pre-amplifier. As a result, the flow noise can be effectively removed by means of balanced detection from the

Optics EXPRESS

microphone pair. The response curve of the PAC as a function of frequency is plotted in Fig. 4.The measured resonance frequency of the PAC was 683.6 Hz with a FWHM of 8.1 Hz in SF_6. A background-gas-induced high-*Q* factor of 85 was observed for SF_6 compared to a *Q*-factor of 20 in N_2, which is in excellent agreement with the theoretical value of 81 and 38 for SF_6 and N_2, respectively. A detailed principle explanation for the background-gas-induced high-*Q* PAC can be found in our previous publication [34].

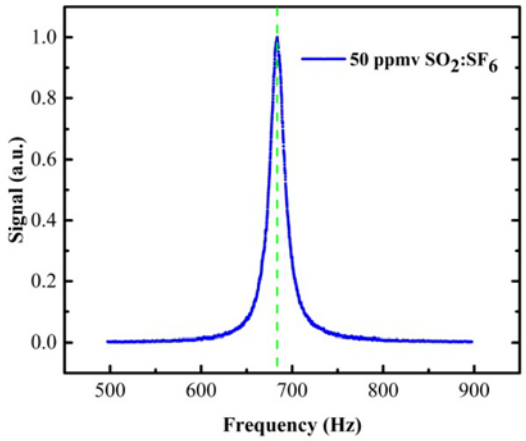

Fig. 4. The response curve of the PAC as a function of frequency. A SO_2:SF_6 mixture was used to generate the photoacoustic signals.

4. Experimental setup of sensor system

A sensitive SO_2 photoacoustic sensor system for the SF_6 decomposition detection was configured on the basis of the differential PAC and the novel DPSSL optical source. The block diagram of the experimental setup is shown in Fig. 5. The differential PAC consists of stainless steel and the internal surface of two resonators was polished. Electrothermal PI film heating elements were used to heat the PAC to a constant temperature of 40 °C in order to minimize adsorption or desorption effects. The CW DPSSL laser was modulated in a semi-pulse mode by a 683.6 Hz square signal with a duty cycle of 50% employing a function generator (Agilent 33210A), which resulted in a mean laser output power of 1.4 mW. The laser beam passed through one of the two resonators to excite the photoacoustic signal, which was detected by the embedded microphone. The second microphone was used to detect the flow noise. These two electret condenser microphones were positioned by means of two adapters flush with the radial resonator surface in a T-configuration [31]. A lock-in amplifier (Stanford SR830) operating in the 1-*f* mode was used to demodulate the differential signal from two microphones. The synchronous signal from the function generator was directed to the lock-in amplifier as the reference signal. A power meter (Ophir Optronics Solutions. LTD, 3A-ROHS) was placed after the PAC to monitor the laser output, since the signal amplitude is directly proportional to the excitation optical power. The result shows a power stability of < ± 5% in a period lasting four hours. The signals from both the lock-in amplifier and power meter were recorded continuously by a computer.

A gas dilution system (Environics EN4000) including four mass flow controllers was used to generate SO_2:SF_6 mixtures from 0 to 50 ppm. The flow and pressure of the gas mixture in the PAC were controlled by a pressure controller (MKS 649B), a needle valve and a diaphragm pump (KNF N813.5ANE). The gas flow rate was measured by a mass flow meter (Alicat M2SLPM), which was placed downstream of the PAC. All experiments were carried out at atmospheric pressure and room temperature.

Optics EXPRESS

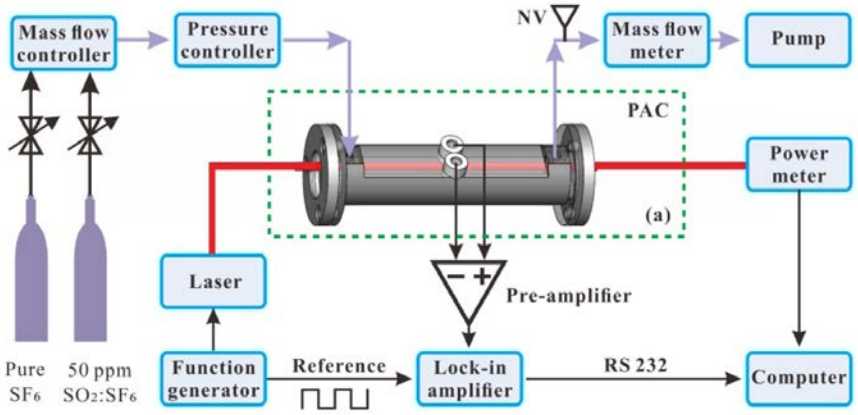

Fig. 5. Schematic of a SO_2 trace gas sensor system in the presence of a SF_6 buffer gas. NV: Needle valve; PAC: photoacoustic cell. (a) a symmetrical differential structure of the PAC.

5. Experimental optimization and evaluation

5.1 Flow noise analysis

The response time of the SO_2 photoacoustic sensor system is determined by two factors. One is the adsorption-desorption processes between SO_2 and the walls, since SO_2 is a polar molecule. The other is the gas-exchange time of the gas sample between the PAC and the electric power system. Precautions were taken to eliminate the adsorption or desorption effects by means of the selection of suitable materials, heating of the walls and application of various surface treatments [35,36]. Moreover, a higher gas flow rate is helpful to reduce the adsorption-desorption effects as well as the gas-exchange time, thereby improving the response time. With the increase of gas flow, the noise level of the photoacoustic sensor system increases sharply. The designed differential PAC's ability to suppress flow noise was assessed.

The signal amplitude (line + square) and noise level (line + circle) of the photoacoustic sensor based on the differential PAC was recorded in the SF_6 flow rate range from 30 sccm to 200 sccm as shown in Fig. 6. The 50 ppm SO_2:SF_6 gas mixture was added into the sensor system and the gas pressure was controlled at 760 Torr. The signal amplitude remained constant within the gas flow rate range, while the noise increased sharply when the flow rate was > 130 sccm. Subsequently, the carrier gas was switched to N_2. The laser modulation frequency was changed to 1783 Hz, matching the resonant frequency of the PAC in N_2. The noise level (line + rhombus) of the sensor system is plotted in Fig. 6. No significant variation of noise level was observed when the gas flow was <800 sccm. This implies that the PAC is more sensitive to the gas flow rate of SF_6 than that of N_2 since SF_6 has a heavier molecular weight. For comparison, the differential PAC was replaced with a single resonator PAC made of the same material, whose resonator has the identical geometrical parameters (Φ6 × 90 mm) with either of the two resonators in the differential PAC. The noise level (line + triangle) of the sensor system in pure SF_6 was recorded. Without balanced detection, the noise level increased sharply when the flow rate was >20 sccm. Therefore, the differential PAC is able to use a 7 times larger SF_6 gas flow than that of a single resonator PAC, which effectively reduce the response time. In the following experiments, a gas flow rate of 100 sccm was selected and the gas exchange time between the PAC and the outside is ~6 s, considering a PAC volume of ~9.8 cm^3.

Optics EXPRESS

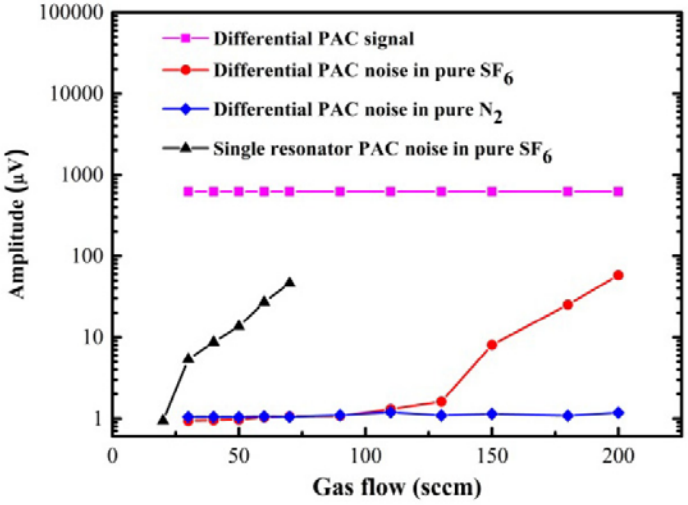

Fig. 6. Dependence of the signal and noise on the gas flow rate within the range of 20-200 sccm. The signal was obtained with 50 ppm SO_2:SF_6 gas mixture. The noise was acquired in pure SF_6 or pure N_2 using either a differential PAC or a single resonator PAC.

5.2 Sensor performance assessment

Different concentrations of the SO_2:SF_6 gas mixtures ranging from 5 ppm to 50 ppm were directed to the PAC in order to assess the sensor detection sensitivity. The response signal amplitudes are shown in Fig. 7(a). The data points were recorded continuously for 100 s with a 1-s averaging time (0.25 Hz bandwidth) after the signal amplitude became constant. A 1σ standard deviation of 0.89 μV was obtained with pure SF_6 gas and this deviation was used as the sensor noise level. The signal amplitude was 60.7 μV with a 5 ppm SO_2:SF_6 gas mixture, which resulted in a signal-to-noise ratio (SNR) of 68. A minimum detection limit of 74 ppbv was obtained, which corresponds to a normalized noise equivalent absorption (NNEA) coefficient of 1.15×10^{-9} $cm^{-1}WHz^{-1/2}$ considering the effective absorption cross-section of 2.1×10^{-19} cm^2/molecule.

In order to verify the linearity of the sensor performance, the average signal amplitudes of 100 data points were plotted in Fig. 7(b) for different gas concentration levels. The linear fitting *R*-Square value >0.9996 confirms the linearity of the sensor response to the SO_2 concentration.

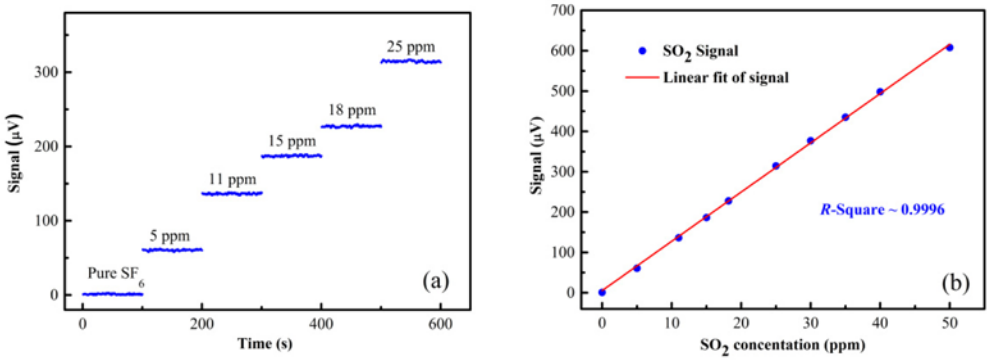

Fig. 7. (a) SO_2 photoacoustic signal amplitudes at different concentrations of SO_2:SF_6 gas mixture within the range of 5-50 ppm. (b) The linearity of the SO_2 photoacoustic senor system.

Optics EXPRESS

6. Conclusions

A ppbv level SO_2 photoacoustic sensor system was developed to detect the SF_6 decomposition in electric power systems. A novel compact DPSSL laser emitting at 303 nm was selected. A fully symmetrical differential PAC was designed to address the issue of the flow noise of SF_6. As a result, the SO_2 photoacoustic sensor can be employed for real-time on-line measurements with a 7 times larger continuous sample gas flow than that with single resonator PAC. The sensor detection limit was further improved by the background-gas-induced high *Q*-factor. A 1σ detection limit of ~74 ppbv was obtained with a 1 s integration time, which corresponds to a NNEA coefficient of 1.15×10^{-9} $cm^{-1}WHz^{-1/2}$. The sensitivity of SO_2 can meet the application requirement of the SF_6 decomposition detection in electric power systems and will be deployed in the future for long time field testing. The sensor's capability can be improved by using a higher excitation optical output power and/or reducing the PAC resonator volume to increase the cell constant.

Funding

This work is supported by National Natural Science Foundation of China (Nos. 61622503, 61575113, 11434007); National Key Research and Development Program of China (No. 2017YFA0304203); Changjiang Scholars and Innovative Research Team in University of Ministry of Education of China (No. IRT13076); Outstanding Innovative Teams of Higher Learning Institutions of Shanxi; Shanxi "1331 Project"key subjects construction. Frank K. Tittel acknowledges support by the US National Science Foundation (NSF) ERC MIRTHE award and the Robert Welch Foundation (Grant #R4925U).

Acknowledgments

We acknowledge the support from Changchun New Industries Optoelectronics Technology Co., Ltd..